ChemComm

Accepted Manuscript

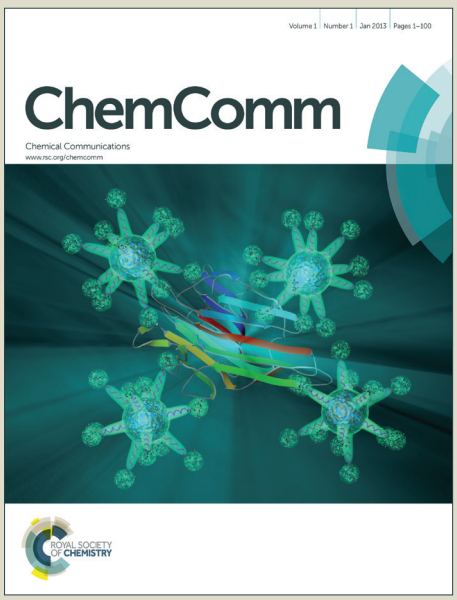

ROYAL SOCIETY OF CHEMISTRY

www.rsc.org/chemcomm

Journal Name

COMMUNICATION

Metal-Organic Frameworks Derived Composites for Cathode Protection: ZrO_2 and Al_2O_3 Coatings of $LiCoO_2$ Derived from UiO-66 and MIL-53 as Ultra-Stable Cathodes in Lithium Ion Batteries

Received 00th January 20xx,
Accepted 00th January 20xx

DOI: 10.1039/x0xx00000x

www.rsc.org/

Pengfei Qi, ‡[a] Yuzhen Han, ‡[a] Junwen Zhou,[b] Xiaotao Fu,[a] Siwu Li,[a] Jingshu Zhao, [a] Lu Wang, [a] Xinxin Fan,[b] Xiao Feng[a] and Bo Wang*[c]

A mechanochemical synthetic method of preparing $LiCoO_2$ coated by MOF-derived metal oxides composites is introduced. Mono-dispersed ZrO_2 and Al_2O_3 are applied as protection layers. These composites show 148 mA h g^{-1} at a current density of 2325 mA g^{-1} and excellent thermal stability (55 °C).

Lithium ion batteries (LIBs) as an important electric energy storage technology in the modern society, have powered various portable electronic devices, and are now providing energy for emergent applications, such as hybrid electric vehicles (HEVs), and electric-vehicles (EVs), due to their relatively high energy density. $LiCoO_2$ is the currently used cathode material in commercial LIBs, which has excellent capacity retention, and high theoretical specific capacity (274 mA h g^{-1}).[1, 2] However, only 56% of the theoretical capacity of $LiCoO_2$ can be practically utilized (155 mA h g^{-1}). Although increasing the voltage is a possible route to raise the energy density of $LiCoO_2$, the decomposition of the electrolyte and the destruction of the space lattice of $LiCoO_2$ are severe problems.[3-6] In addition, inferior rate-performance and thermostability are further drawbacks to be overcome for the optimization of $LiCoO_2$-based LIBs.[7, 8]

One available approach is to adopt surface modifications for $LiCoO_2$ with a protecting layer, such as Al_2O_3, ZrO_2 and so on.[9-12] These agents can protect $LiCoO_2$ from the attack by HF generated during operation and suppress the lattice changes of $LiCoO_2$;[13-15] both are beneficial for mitigating the structural deformation of $LiCoO_2$. Albeit considerable improvements on the cycling stability of $LiCoO_2$, the advantage of this approach is offset by the penalties on specific capacity and rate capability caused by the poorly conductive coating layer. Thus, to minimize the use of these insulating components without sacrificing their stabilizing functions is the key challenge for the construction of a more effective coating layer. Besides, suitable porosity across the layer is also desirable to enable fast kinetics for Li^+ transport.[16, 17]

Metal–organic frameworks (MOFs) are a class of highly porous materials assembled by the coordination of metal ions and organic ligands, with tremendous variety and flexibility of type, structure and functionality.[18-20] Recent research shows that MOFs can be ideal precursors to produce functional hybrid materials with attractive properties in electrochemical applications. .[21-23] In this paper, we fabricated multifunctional surface coatings for $LiCoO_2$ via calcinations of two distinct MOFs, UiO-66 and MIL-53 (for detailed experimental procedures please see ESI). The results show that ZrO_2 and Al_2O_3 can be mono-dispersed across the porous carbon frameworks derived from UiO-66 and MIL-53, respectively, serving as protecting agents for $LiCoO_2$. These protected $LiCoO_2$ composites as active cathode materials show impressive cycle performance especially at high current density (148 mA h g^{-1} at a current density of 2325 mA g^{-1}) and excellent thermal stability at elevated temperature (55 °C). It is also shown that these MOF-derived protection layers can effectively alleviate the structural change of $LiCoO_2$ and hence improve its electrochemical performance at extreme conditions.

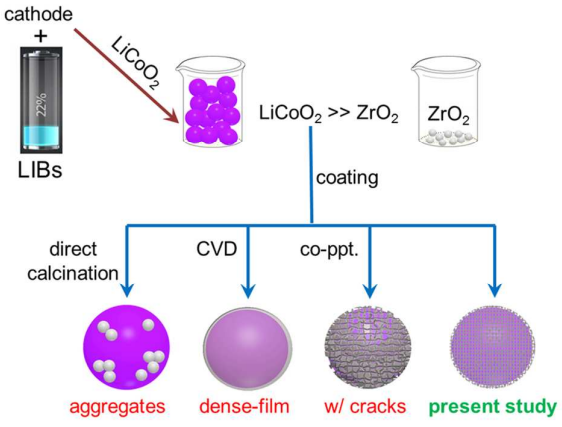

Fig. 1 Different routes to coat $LiCoO_2$ (co-ppt denotes co-precipitation).

[a] *Key Laboratory of Cluster Science, Ministry of Education of China, Beijing Key Laboratory of Photoelectronic/Electrophotonic Conversion Materials, School of Chemistry, Beijing Institute of Technology, Beijing 100081, P. R. China.*
[b] *College of Chemistry and Molecular Engineering, Peking University, 5 Yiheyuan Road, Beijing 100871, P.R. China*
[c] *E-mail: bowang@bit.edu.cn;*
† Electronic Supplementary Information (ESI) available: Synthetic materials and instruments, synthetic methods, and experimental are included in the supporting information. See DOI: 10.1039/b000000x/
‡ These authors contributed equally to this work.

ZrO_2 and Al_2O_3, as metal oxides, are commonly used coating materials for $LiCoO_2$. The coating can be achieved through many routes. The simplest method, for example, is to mingle the powders of $LiCoO_2$ with ZrO_2 (or Al_2O_3). Yet poorly dispersed ZrO_2 (or Al_2O_3) aggregates are formed on the surfaces of $LiCoO_2$, leaving plenty of unprotected regions. Another type of coating is given by CVD, through which a dense and continuous layer fully covers the whole surface of the $LiCoO_2$ particle; the non-conductive and non-porous coating layer remarkably hinders the transfer of both Li-ions and electrons across the interface, undermining the activity of $LiCoO_2$.[10, 11, 24] Co-precipitation (co-ppt.) method can also coat $LiCoO_2$ with ZrO_2 (or Al_2O_3), providing, however, irregular and incomplete coverage with cracks; aggregates in this case cannot be avoided.[25] In our approach, Zr^{4+} (or Al^{3+}) ions are initially constructed in the crystalline framework of UiO-66 (or MIL-53). After the mechanochemical and the following thermal process of $LiCoO_2$ with UiO-66 (or MIL-53), well-dispersed particles of ZrO_2 (or Al_2O_3) uniformly distributes on the surface of $LiCoO_2$, with channels allowing for the access to the conductive matrix and the transport of Li-ions (Fig. 1).

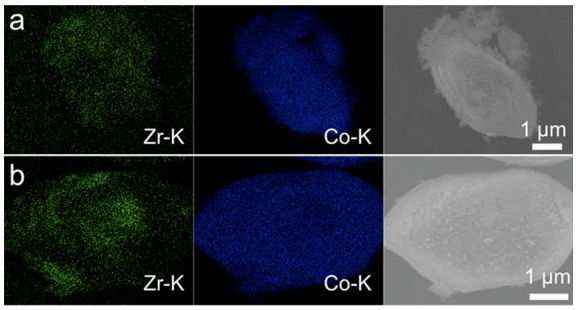

Fig. 2 EDS mappings and SEM images of (a) UiO-66@$LiCoO_2$-600 and (b) ZrO_2@$LiCoO_2$-600 ((a) and (b) stand for "present study" and "aggregates" in **Fig. 1**, respectively).

To illustrate the advantages of using MOFs as precursors for surface modification, we treated $LiCoO_2$ via the same mechanical and thermal procedure with both MOFs (UiO-66 or MIL-53, denoted as "MOF-derived coating") and their resulting oxides (ZrO_2 or Al_2O_3, denoted as "oxide coating"). The structural evolution of the two MOFs upon calcination was first studied by powder X-ray diffraction (PXRD, Fig. S1, S2, S3 & S4). The diffraction peaks of UiO-66 or MIL-53 vanish after the 600 °C treatment in air; instead, peaks attributive to two different crystal phases of ZrO_2 (PDF # 65-1022 and PDF # 65-0461) or Al_2O_3 (PDF # 49-0134), respectively, appear in the patterns, with substantial broadening. These results indicate that highly dispersed oxides with restricted crystalline grain size are derived after calcinations thanks to the MOF precursors. The nitrogen sorption isotherms and pore size distributions of UiO-66-600 and MIL-53-600 are shown in Fig. S5 and Fig. S6 in the ESI. UiO-66-600 has a Brunauer–Emmett–Teller (BET) specific surface area of 117 $m^2\ g^{-1}$ and a narrow pore size distribution around 2.5-25 nm (for MIL-53-600: BET specific surface area of 173 $m^2\ g^{-1}$ and pore size about 2-25 nm). In $LiCoO_2$ with MOF-derived and oxide coatings, due to the minor addition of UiO-66 and ZrO_2, respectively, only $LiCoO_2$ can be obviously detected under PXRD in UiO-66@$LiCoO_2$-600 (before cycling) and ZrO_2@$LiCoO_2$-600 (before cycling), as shown in Fig. 3a. Similar results were obtain with MIL-53 and bare Al_2O_3 (Fig. S7). The existence of UiO-66 (or MIL-53) on the surfaces of $LiCoO_2$ was thus verified by FT-IR spectroscopy. Both the $\nu_{C=O}$ and $\nu_{C=C}$ (in the benzene ring) can be observed at 1706 cm^{-1} and 1480 cm^{-1}, respectively, absent in the bare $LiCoO_2$ sample (Fig. S8).[26]

Surface roughness of the treated $LiCoO_2$ samples increases in comparison with the bare one, as shown in SEM (Fig. 2, S9, S10 and S11). The major difference in a MOF-derived coating comparing to the oxide counterpart, however, is the spatial distribution of Zr (or Al) element within the treated $LiCoO_2$ samples. This information was obtained by elemental mapping under SEM. As shown in Fig. 2, Zr in UiO-66@$LiCoO_2$-600 uniformly distributes on the surface of $LiCoO_2$, while Zr in ZrO_2@$LiCoO_2$-600 does not, remaining aggregates of hundreds of nanometers in size. The comparison between MIL-53@$LiCoO_2$-600 and Al_2O_3@$LiCoO_2$-600 gives similar results (Fig. S10). Clearly, MOF-derived coatings enable more uniform distribution of ZrO_2 or Al_2O_3, thus more complete protection on the surfaces of $LiCoO_2$. (The concentration of zirconia (or alumina) was small, typically less than the 1 wt. %, calculated from elemental analysis by ICP (Inductive Coupled Plasma Emission Spectrometer). Some zirconia seems to have penetrated deep into the bulk of the $LiCoO_2$ particles during the calcination process.[27])

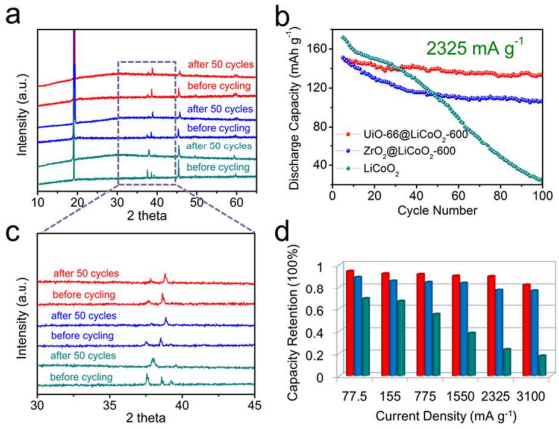

Fig. 3 (a) PXRD of UiO-66@$LiCoO_2$-600 (red line), ZrO_2@$LiCoO_2$-600 (blue line) and $LiCoO_2$ (dark cyan line). (b) Cycling performance of UiO-66@$LiCoO_2$-600, ZrO_2@$LiCoO_2$-600 and $LiCoO_2$ between 3.0 and 4.5 V at a current density of 2325 mA g^{-1}. (c) PXRD of UiO-66@$LiCoO_2$-600, ZrO_2@$LiCoO_2$-600 and $LiCoO_2$ (2theta: 30 – 45 degree). (d) Capacity retention for UiO-66@$LiCoO_2$-600 (red column), ZrO_2@$LiCoO_2$-600 (blue column) and $LiCoO_2$ (dark cyan column) at different current densities.

To study the effects of different coatings on the electrochemical performance of $LiCoO_2$ cathodes, coin cells with Li metal were assembled. Galvanostatic tests on the coated $LiCoO_2$ as well as the bare one were conducted at various current densities between 3.0 and 4.5 V. In all situations, batteries were activated at 77.5 mA g^{-1} for the first four cycles.

Fig. 3b shows the cycling performance at a current density of 2325 mA g^{-1} (2325 mA g^{-1} corresponds to a full discharge/charge within 5 min). Surface coatings generally lead to slightly lowered initial capacity at 2325 mA g^{-1}, from 170 mA h g^{-1} (bare) to 148 (UiO-66@$LiCoO_2$-600) and 149 mA h g^{-1} (ZrO_2@$LiCoO_2$-600), due to the increased resistance resulted from the coatings(Fig. S12). Cycling stability, however, enhances substantially after surface coatings. Comparing to the ultra-low retention of 12.9% over 100 cycles given

by the bare $LiCoO_2$, ZrO_2@$LiCoO_2$-600 achieves a retention of 71.1%. UiO-66@$LiCoO_2$-600, strikingly, stands at 134 mA h g^{-1} after 100 cycles at 2325 mA g^{-1}, corresponding to an exceptional retention level of 89.5%! MIL-53@$LiCoO_2$-600 also shows higher cycling stability at 2325 mA g^{-1} than its oxide counterpart, Al_2O_3@$LiCoO_2$-600 (Fig. S13), with capacity retention over 100 cycles of 79.6% and 72.8%, respectively. Under all current densities (77.5, 155, 775, 1550, 2325 and 3100 mA g^{-1}) and different rates of 1 C and 5 C (1 C = 180 mA g^{-1}), MOF-derived coatings outperform their oxide counterparts (Fig. 3d, Fig. S14, Fig. S15 and Fig. S16), indicating the strong stabilizing effects given by the unique coating structures.

When cycled at a cutoff voltage above 4.1 V vs. Li^+/Li, $LiCoO_2$ cathode often undergoes a clear phase transition (hexagonal–monoclinic–hexagonal), which leads to its deteriorated electrochemical performance.[28, 29] This phase transition is accompanied by a 1.2% expansion in the c-direction and 9% in volume change,[30] and consequently causes cracks in the particles, reducing the cyclability.[28] In order to understand the underlying mechanism of the stabilizing effects given by the MOF-derived coatings, PXRD were conducted for the cathode materials after 50 cycles at 2325 mA g^{-1}. Without any surprise, diffraction peaks between 36 to 40° change in ZrO_2@$LiCoO_2$-600 and $LiCoO_2$, indicating a transformation from the original hexagonal phase to the monoclinic phase (Fig. 3a and 3c).[31, 32] In contrast, the PXRD pattern of UiO-66@$LiCoO_2$-600 remains intact. These results explicitly demonstrate that the structural degradation of $LiCoO_2$ is effectively suppressed by the MOF-derived coating layer.[33] As a result, the resulting cathode material is able to stably operate at extreme rates.

To further examine the stability of the modified $LiCoO_2$ material, we also tested the batteries under 155 mA g^{-1} at an elevated temperature of 55 °C (Fig. 4). UiO-66@$LiCoO_2$-600, ZrO_2@$LiCoO_2$-600, and $LiCoO_2$ release similar initial capacities (~ 173 mA h g^{-1}). After 100 cycles, however, obvious difference takes place in capacity retention. The capacity of $LiCoO_2$ drops quickly to about 125 mA h g^{-1}, and 132 mA h g^{-1} for ZrO_2@$LiCoO_2$-600. Encouragingly, UiO-66@$LiCoO_2$-600 still maintains at a high level of 147 mA h g^{-1}, corresponding to a capacity retention of 84.8%. This valued feature enables wider operational temperature for the batteries.

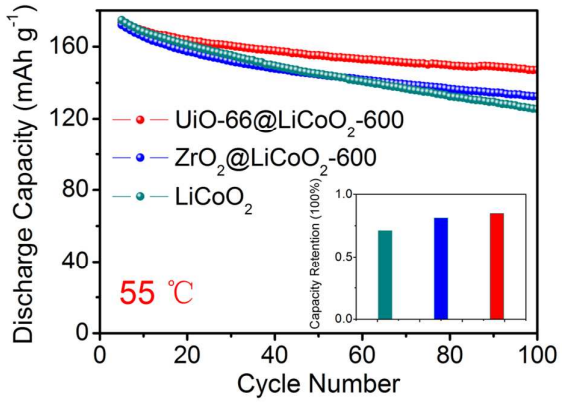

Fig. 4 Cycling performance of UiO-66@$LiCoO_2$-600, ZrO_2@$LiCoO_2$-600 and $LiCoO_2$ between 3.0 and 4.5 V under 155 mA g^{-1} at 55 °C. The cells were activated at the current density of 77.5 mA g^{-1} for four cycles. The insert figure stands for capacity retention of $LiCoO_2$ (dark cyan bar), ZrO_2@$LiCoO_2$-600 (blue bar), UiO-66@$LiCoO_2$-600 (red bar).

In summary, we have demonstrated a convenient route to build up an effective protecting layer for $LiCoO_2$ derived from MOFs through a simple mechanochemical treatment in conjunction with calcinations. The modified $LiCoO_2$ shows impressive rate performance and thermal stability. 148 mA h g^{-1} can be achieved at 2325 mA g^{-1} with excellent retention of 90.5% over 100 cycles. 85.0% of the initial capacity can be retained after a 100-cycle galvanostatic test under 155 mA g^{-1} at 55 °C. By virtue of general and facial synthetic approach and outstanding electrochemical performance, this work may shed light on the development of traditional cathode materials with MOF-derived modifications. Further research on improving the electrical conductivity of the coating layer and the overall capacity is still in process and the results will be reported soon.

This work was financially supported by the 973 Program 2013CB834704; Provincial Key Project of China (7131253); the National Natural Science Foundation of China (21471018, 21201018, 21404010); 1000 Plan (Youth).

Notes and references

1. J. B. Goodenough, *Accounts Chem. Res.*, 2013, **46**, 1053-1061.
2. M. Jo, S. Jeong and J. Cho, *Electrochem. Commun.*, 2010, **12**, 992-995.
3. T. Takeuchi, T. Kyuna, H. Morimoto and S.-i. Tobishima, *J. Power Sources*, 2011, **196**, 2790-2801.
4. A. Sakuda, A. Hayashi and M. Tatsumisago, *J. Power Sources*, 2010, **195**, 599-603.
5. Z. Wang, Z. Wang, H. Guo, W. Peng and X. Li, *J. Alloy. Compd.*, 2015, **626**, 228-233.
6. Z. Yang, W. Yang, D. G. Evans, G. Li and Y. Zhao, *Electrochem. Commun.*, 2008, **10**, 1136-1139.
7. J. P. Cho and G. Kim, *Electrochem. Solid St.*, 1999, **2**, 253-255.
8. J. Cho, Y. J. Kim and B. Park, *Chem. Mater.*, 2000, **12**, 3788-3791.
9. E. Jung and Y. J. Park, *J. Electroceram.*, 2012, **29**, 23-28.
10. J. H. Woo, J. E. Trevey, A. S. Cavanagh, Y. S. Choi, S. C. Kim, S. M. George, K. H. Oh and S. H. Lee, *J. Electrochem. Soc.*, 2012, **159**, A1120-A1124.
11. X. Dai, L. Wang, J. Xu, Y. Wang, A. Zhou and J. Li, *ACS Appl. Mater. Interfaces*, 2014, **6**, 15853-15859.
12. H. Lee, H.-J. Kim, D. Kim and S. Choi, *J. Power Sources*, 2008, **176**, 359-362.
13. Y. J. Kim, T.-J. Kim, J. W. Shin, B. Park and J. Cho, *J. Electrochem. Soc.*, 2002, **149**, A1337.
14. Y. J. Kim, J. Cho, T.-J. Kim and B. Park, *J. Electrochem. Soc.*, 2003, **150**, A1723.
15. J. Cho, T.-G. Kim, C. Kim, J.-G. Lee, Y.-W. Kim and B. Park, *J. Power Sources*, 2005, **146**, 58-64.
16. T. Loiseau, C. Serre, C. Huguenard, G. Fink, F. Taulelle, M. Henry, T. Bataille and G. Ferey, *Chem. - Eur. J.*, 2004, **10**, 1373-1382.

17. J. H. Cavka, S. Jakobsen, U. Olsbye, N. Guillou, C. Lamberti, S. Bordiga and K. P. Lillerud, *J. Am. Chem. Soc.*, 2008, **130**, 13850-13851.
18. H. Furukawa, K. E. Cordova, M. O'Keeffe and O. M. Yaghi, *Science*, 2013, **341**, 1230444.
19. B. Wang, A. P. Cote, H. Furukawa, M. O'Keeffe and O. M. Yaghi, *Nature*, 2008, **453**, 207-211.
20. Y. Guo, X. Feng, T. Han, S. Wang, Z. Lin, Y. Dong and B. Wang, *J. Am. Chem. Soc.*, 2014, **136**, 15485-15488.
21. H. L. Jiang, B. Liu, Y. Q. Lan, K. Kuratani, T. Akita, H. Shioyama, F. Zong and Q. Xu, *J. Am. Chem. Soc.*, 2011, **133**, 11854-11857.
22. Y. Han, P. Qi, S. Li, X. Feng, J. Zhou, H. Li, S. Su, X. Li and B. Wang, *Chem. Commun.*, 2014, **50**, 8057-8060.
23. Y. Han, P. Qi, X. Feng, S. Li, X. Fu, H. Li, Y. Chen, J. Zhou, X. Li and B. Wang, *ACS Appl. Mater. Interfaces*, 2015, **7**, 2178-2182.
24. S.-M. Moon, W. Chang, D. Byun and J. K. Lee, *Curr. Appl. Phys.*, 2010, **10**, e122-e126.
25. W. Luo, X. Li and J. R. Dahn, *J. Electrochem. Soc.*, 2010, **157**, A782.
26. M. Kandiah, S. Usseglio, S. Svelle, U. Olsbye, K. P. Lillerud and M. Tilset, *J. Mater. Chem.*, 2010, **20**, 9848-9851.
27. Z. H. Chen and J. R. Dahn, *Electrochim. Acta*, 2004, **49**, 1079-1090.
28. H. F. Wang, Y. I. Jang, B. Y. Huang, D. R. Sadoway and Y. T. Chiang, *J. Electrochem. Soc.*, 1999, **146**, 473-480.
29. E. Plichta, S. Slane, M. Uchiyama, M. Salomon, D. Chua, W. B. Ebner and H. W. Lin, *J. Electrochem. Soc.*, 1989, **136**, 1865-1869.
30. K. Dokko, M. Nishizawa, S. Horikoshi, T. Itoh, M. Mohamedi and I. Uchida, *Electrochem. Solid St.*, 2000, **3**, 125-127.
31. J. Cho, Y. J. Kim, T. J. Kim and B. Park, *Angew. Chem., Int. Ed.*, 2001, **40**, 3367-3369.
32. T. Ohzuku and A. Ueda, *J. Electrochem. Soc.*, 1994, **141**, 2972-2977.
33. J. Cho, B. Kim, J.-G. Lee, Y.-W. Kim and B. Park, *J. Electrochem. Soc.*, 2005, **152**, A32.